Chapter 6

Novel thermoplastic bonding using bulk metallic glass solder

A novel thermoplastic bonding concept is demonstrated based on the unique rheological behavior and pattern-replication ability of bulk metallic glass forming liquids. In this approach, the bulk metallic glass is heated above T_g to the “supercooled liquid” region while a small normal force is applied to the joint. This results in liquid reflow, wetting and a strong bond. Complete wetting between copper substrates and a layer of platinum based bulk metallic glass leads to an atomistically intimate void-free interface.

6.1 Introduction

One of the characteristics of Bulk Metallic Glass (BMG) is the existence of a supercooled liquid region between glass transition (T_g) and crystallization (T_x) temperatures on heating. In the supercooled liquid state, the atomic configuration of the BMG easily rearranges to accommodate plastic flow. Supercooled liquids, depending on their fragility, can have sufficient fluidity to flow under small applied pressure. The viscosity of supercooled liquids of BMGs is known to be as low as 6×10^4 Pa·s, similar to that of viscous polymer melts [1]. The fluidity of a supercooled BMG forming liquid also makes micron-sized pattern replication possible [2]. Thus it is reasonable to expect that the supercooled BMG forming liquid can wet and bond to another metal surface during this configurational rearrangement process. In this chapter, a series of bonding experiments were performed to demonstrate this new concept of thermoplastic bonding using BMG alloys. Interfacial integrity and fracture behavior are also studied.

6.2 Motivations and possible application to microelectronics industry

Solders have been extensively used in microelectronics industry because of their desirable properties such as low melting temperature (T_m) and high ductility which permits flow and reduces stress on adjacent components. Solders also exhibit good wetting on high-conductivity metal contacts like copper. Despite these attractive properties, conventional soldering has fundamental limitations. First, soldering is mainly based on reactive wetting and the reaction by-product is often a brittle intermetallic compound (IMC). The deleterious effect of IMC formation on long-term reliability of solder joints has been well documented [3-6]. Second, soldering temperature is fundamentally coupled with T_m of the solder. As a result, low-T_m solders must typically be used for low-temperature assembly where heat-sensitive devices (such as

ferroelectric polymers or liquid crystals) are to be assembled. However, such low-T_m solders are inevitably subject to high homologous temperatures (T_{hom}) in final service. Therefore they suffer extensive creep, strength loss and poor thermal stability over time. In turn, this limits their long-term reliability [7].

In this study, a novel joining/bonding concept, "thermoplastic soldering" is reported based on the unique rheological behavior [1,8] and pattern-replication ability of Bulk Metallic Glasses (BMG) [2]. BMG thermoplastic soldering provides a novel way to achieve metallurgical joining/bonding according to the following considerations:

1. On heating, BMG becomes a supercooled liquid between glass transition (T_g) and crystallization (T_x) temperatures. In the thermoplastic soldering approach, wetting takes place in the supercooled liquid state as opposed to molten state above T_m in the case of conventional soldering (see Figure 6-1). Supercooled liquids, depending on their fragility, can have sufficient fluidity to reflow under minor pressure. The fluidity of supercooled liquids of bulk metallic glasses is comparable to thermoplastics during plastic injection molding [1]. Therefore bulk metallic glass solders can be viewed as thermoplastic solders.

2. In thermoplastic soldering, the soldering temperature (~T_g) is "decoupled" from T_m. Therefore low temperature thermoplastic soldering can be achieved at relatively low process temperature compared to T_m. This potentially leads to superior reliability. After bonding, a wide variety of nano-/micro-structures from fully amorphous to partially-crystallized, to fully-crystallized structures can be obtained as a final state by controlling crystallization via post-bonding annealing to tailor the optimum electrical conductivity, creep resistance and fatigue properties for a given application. Considering the ultimate tensile strength of current Sn-based solders is around 50 MPa [9, 10], even embrittled or crystallized BMG solder could be considered for such applications. This leads to a lower homologous temperature (T_{hom}) in final service.

Therefore, joints fabricated using this method would be more resistant to creep, electromigration, strength loss and poor thermal stability over time.

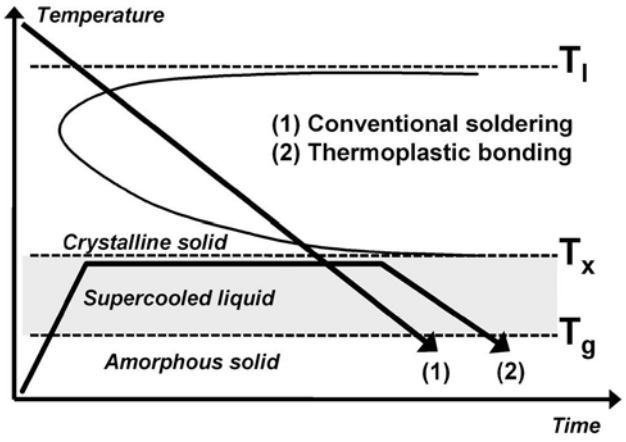

Figure 6-1. Schematic diagram showing the concept of "*Thermoplastic bonding.*"

6.3 Proof of concept experiment (Effect of processing condition)

6.3.1 Experimental

In order to demonstrate this novel bonding concept, a platinum based BMG [11] was selected because of its oxygen inertness and low T_g. A fully amorphous strip of $Pt_{57.5}Cu_{14.7}Ni_{5.3}P_{22.5}$ [11] with thickness of about 0.46 mm was prepared with T_m, T_g and T_x of 499, 226.1 and 299.2°C, respectively (measured by a Netzsch 404C DSC at a scan rate of 20°C-min^{-1}.). Copper cylinders of 6.35mm diameter, 6.35mm length and purity of 99.996% (produced by Alfa Aesar) were used as substrates. Machining reduced the diameter at the bonding surface to 3mm by having the surface outside this 'contact zone' slightly slanted to about 2-3 degrees from horizontal line, as shown in the inset in Figure 6-2. The cylinders were dipped into nitric acid to

remove any surface oxide on the copper. The glassy solder strip was stacked between two copper cylinders without flux, and the assembly was placed in a loading fixture inside a vacuum chamber equipped with a Radio Frequency (RF) heating coil. Temperature was monitored via a K-type thermocouple spotwelded to one of the copper cylinders. The bonding process was performed in a high vacuum of order 10^{-6} mbar to minimize any oxidation. The assembly stack was heated to the process temperature at a heating rate of approximately 100°C-min^{-1}, held at the process temperature under load for 2 minutes, then cooled. Figure 6-2 shows a joint formed by the BMG supercooled liquid bonding process.

After bonding, the electrical resistance of each joint was measured using the 4-point probe method with an approximately 5mm inner probe spacing. The bond strength was measured mechanically using an Instron 5500R frame with a constant crosshead speed of 0.2mm-min^{-1}. Fracture surfaces were examined using a Leo 1550 VP Field Emission SEM.

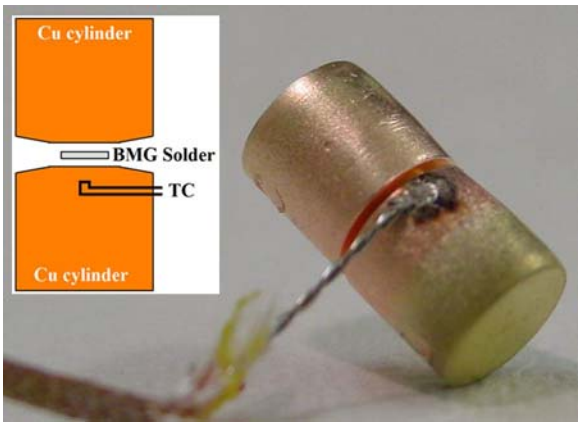

Figure 6-2. Copper-solder-copper stack with thermocouple after processing. Inset: schematic diagram showing experimental configuration.

6.3.2 Results and Discussions

Three different process loads were used for bonding: 5.4, 14.2 and 36.5N, respectively. With the 7.065mm^2 bonding area (area of the 'contact zone' with 3mm diameter), this correlates to an applied pressure of 0.76, 2.0 and 5.2 MPa. And, two different temperatures, 290 and 300°C, were used for the process. A stable, homogeneous joint was not formed at the lowest load, 5.4N. Thus, it is evident that a minimum process load is necessary for joint formation. Once the process load exceeds this critical threshold, the effect of additional load on joint integrity appears to be insignificant. Failure load of joints generated at process loads of 14.2 and 36.5N are shown in Table 6-1. The failure loads of joints formed at 290°C with 14.2 and 36.5N preload are 152 and 122N, respectively. Failure loads for joints formed at 300°C are 319 and 354N.

Table 6-1. Bonding process condition and experimental results.

Process load (N)	Process temp (°C)	Solder weight (mg)	Solder dia. after process (mm)	Solder thickness after process (μm)	Fracture load (N)	Stress with 3mm-dia. bonding area (MPa)	Stress with actual dia. of sample after process (MPa)
14.2	290	25.34	4.35	95.04	151.9	21.5	10.2
14.2	300	19.35	4.43	64.07	318.5	45.1	20.7
36.5	290	13.83	3.99	62.45	121.5	17.2	9.7
36.5	300	15.01	4.28	53.14	353.8	50.0	24.6

The final thickness of BMG solder after process is calculated using solder weight, solder diameter measured after process (given in Table 6-1) and solder density (15.3 g/cc) [12] taking the slope of the surface outside the 'contact zone' into account. Initially 460μm thick solders

were squeezed down to between 50 and 100μm indicating significant flow in each solder during process.

The fracture surfaces examined using SEM back-scattered images of separated joints processed with 36.5N load are shown in Figure 6-3. The samples in Figure 6-3(a-1) and (a-2) were formed at 290°C and Figure 6-3(b-1) and (b-2) at 300°C. Circles in each micrograph indicate the 3mm diameter ‘contact zone’. From compositional contrast, the copper surface appears dark and the platinum based BMG surface bright. Comparing the surfaces in figures (a) and (b), we see that the failure mode transitions from Cu/BMG interfacial fracture to fracture within the BMG solder as the process temperature increases. For the joint produced at 290°C, only a small fraction of the ‘contact zone’ has BMG solder residue on the copper surface (Fig. 6-3(a-1)). On the other hand, for the joint processed at 300°C, most of the ‘contact zone’ is covered by BMG solder residue (Fig. 6-3(b-1)).

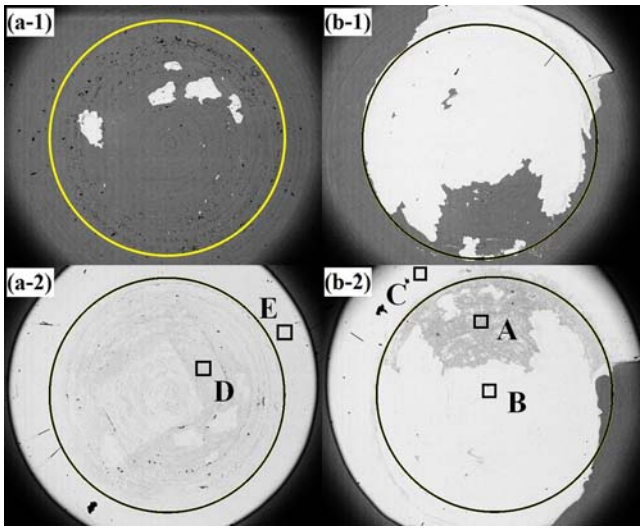

Figure 6-3. Back scattered images of both fracture surfaces of joints produced with 36.5N at (a) 290°C and (b) 300°C. By the compositional contrast, copper surface looks dark and platinum based BMG surface looks bright. The circle marks show ‘contact zone’ with 3-mm diameter. Squared areas marked as from A to E indicate where EDS scans were performed. (listed in Table 6-2.)

Table 6-2. Compositional information by Energy Dispersive Spectroscopy (in at.%).

Area	Pt	Cu	Ni	P
A	20.8	72.8	1.5	4.9
B	60.3	19.9	5.5	14.3
C	57.5	19.7	5.9	16.9
D	37.7	51.1	3	8.2
E	58.1	18.8	4.9	18.2

Energy Dispersive Spectroscopy (EDS) data acquired from squared areas defined in Figure 6-3 are summarized in Table 6-2. For the sample processed at 300°C, as expected from the contrast given by back-scattered electron image, the shaded area (around square A in Figure 6-3(b-2)) has a significantly high concentration of copper. This area was in contact with copper substrate before fracture. The large amount of copper residue on the detached BMG solder surface must be related to the strong bond formation. Bright area (around square B) is a fracture surface of BMG solder. Because this part was distant from the interface with copper, EDS shows almost identical composition with known composition of the solder used. The area outside the circle (around square C) shows that concentration of copper was not increased thereby indicating that the area outside the 'contact zone' did not form a strong bond interface. The same tendency was acquired from the sample processed at 290°C (squares D and E in Figure 6-3(a-2)). This is also confirmed by the fact that the shaded area in both Figure 6-3(a-2) and (b-2) is limited inside the 'contact zone'. This is because the fluid pressure squeezed between parallel plates is decreasing as a function of r, distance from center [13]. And, the slope outside the 'contact zone' should cause an additional pressure drop which could result in poor bonding quality in this area. Thus, it might be reasonable to evaluate the fracture stress of the joints based on the area of the 'contact zone'. As shown by Table 6-1, failure stress of joints formed at 290°C with 14.2 and 36.5N preload, calculated based on 7.065mm^2 contact area, are 21.5 and 17.2MPa, respectively. Failure stress for joints formed at 300°C are 45.1 and 50.0MPa. Also, stress calculated by the whole surface area of each solder, which is the lowest limit value for bonding stress, is given in Table 6-1.

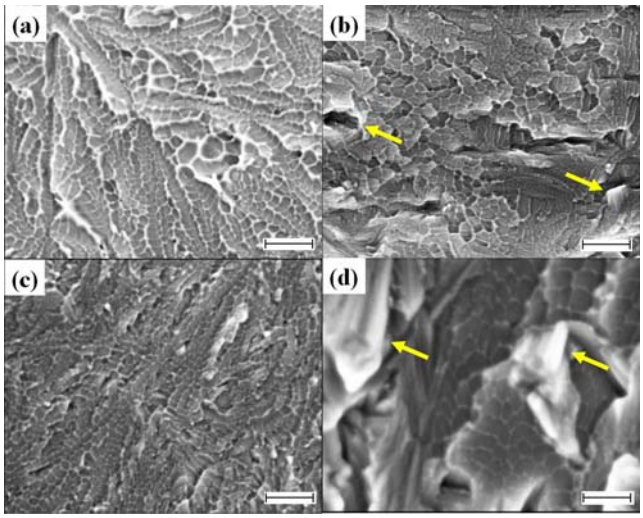

Figure 6-4. High resolution fractography on BMG solder residues produced by (a) 36.5N at 290°C, (b) 36.5N at 300°C, (c) 14.2N at 290°C and (d) 14.2N at 300°C. Scale bars in (a-c) for 200 nm (100,000× magnification) and (d) for 100 nm (200,000× magnification).

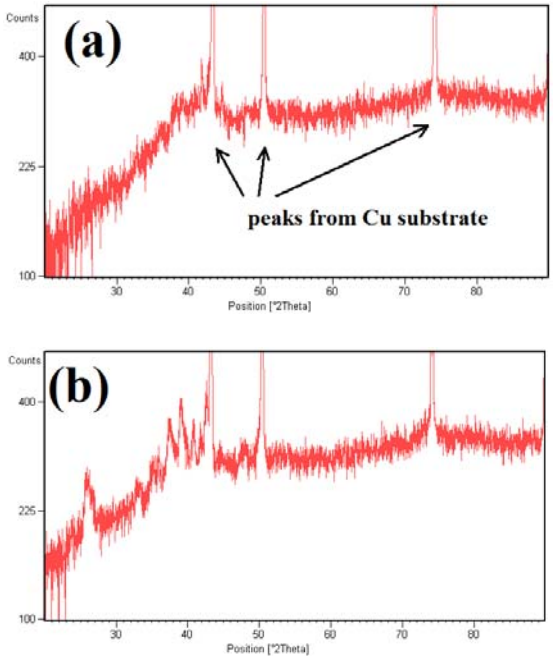

Figure 6-5. X-ray diffraction patterns of fracture surface of joints produced with 36.5N at (a) 290°C (surface shown in Figure 6-3(a-2)) and (b) 300°C (surface shown in Figure 6-3(b-2)).

High resolution fractography of the BMG solder residues reveals a dimple pattern (Figure 6-4). This dimple pattern is typical for fracture surfaces of BMGs [14, 15] and confirms that fracture is through the BMG and not along the interface. For both joints, the areas with BMG solder residue are thought to have formed an intimate interface between the copper and BMG solder. It is also notable that the size of dimple is less than 100 nm for both samples processed at 290 and 300°C. According to an empirical relationship regarding the dimple size [15], small dimple size correlates with poor fracture toughness. In addition, small crystallites growing with a columnar shape are shown in the sample processed at 300°C (indicated by arrows in Figure 6-4(b) and (d)). This crystallization also can be confirmed by X-ray diffraction pattern shown in Figure 6-5. Figure 6-5(a) is taken from a surface shown in Figure 6-3(a-2) which is formed at 290°C and Figure 6-5(b) from Figure 6-3(b-2) at 300°C. Except for the peaks from Cu substrates, the pattern taken from the solder surface processed at 290°C (Figure 6-5(a)) appears glassy. On the other hand, the surface processed at 300°C, shown in Figure 6-5(b), shows many crystalline peaks. Generally crystallization of a BMG is known to accompany embrittlement. Due to the process temperatures being as high as the crystallization temperature, crystallization to a certain extent during processing appears to be inevitable for the current Pt-based BMG and copper system. Thus, additional study is required to understand the details of the bonding mechanism. A better understanding of the bonding mechanism could lead to enhanced wettability of BMG solders at lower temperature, improved interfacial integrity and increased control over the final structure of the BMG solder.

As shown in Table 6-1, the final thickness of the BMG solders ranges from 50 to 100 μm. The measured electrical resistance of the joints is reasonably small, ranging from 21 to 27μΩ for the joints formed at 290°C and from 13 to 15μΩ for those at 300°C. For the joints formed at 300°C, an ideal resistance is estimated for a 50μm thick BMG solder with an area of 7.065mm^2 to

be 13.1μΩ based on the resistivity of the platinum based glass (1850nΩ·m). The measured resistance values are close enough to claim formation of an intimate interface.

6.4 Cross-sectional Transmission Electron Microscopy (TEM) study

For cross-sectional TEM work, joints were sectioned via ultramicrotomy and examined using an FEI Tecnai F30UT high resolution TEM operated at 300kV.

Figure 6-6 shows TEM images of the specimen shown in Figure 6-3(b), which is processed at 300°C with 36.5 N. The BMG solder is partially crystallized as seen in Figure 6-4 and 6-5. The spot pattern shows amorphous ring and many tiny dots on the amorphous hollow, which suggests the existence of small crystalline particles (Figure 6-6(a)). A pair of bright field and dark field images (Figure 6-6(b) and (c)) shows nano-meter sized crystalline particles inside the BMG solder. Although most of the BMG solder is partially crystallized, an intimate interface between copper substrate and BMG solder can be found as shown in Figure 6-7.

An interface processed at temperature lower than 300°C is also observed. Cross-sectional TEM observations of the interface shown in Figure 6-8(a) and (b) shows that the BMG solder completely replicates microscopic details of the copper surface and forms a void-free interface. High resolution imaging of the interface (Figure 6-8(c)) provides evidence that the BMG solder forms an intimate atomistic scale bond with the copper. No interfacial reaction product is observed along the interface between BMG and copper within the resolution of the TEM.

Stepwise EDS spectrum scan performed from the interface to about 1.5 μm deep into the Pt-BMG with a 0.1 μm step size does not find any evidence of preferred diffusion of specific constituting element.

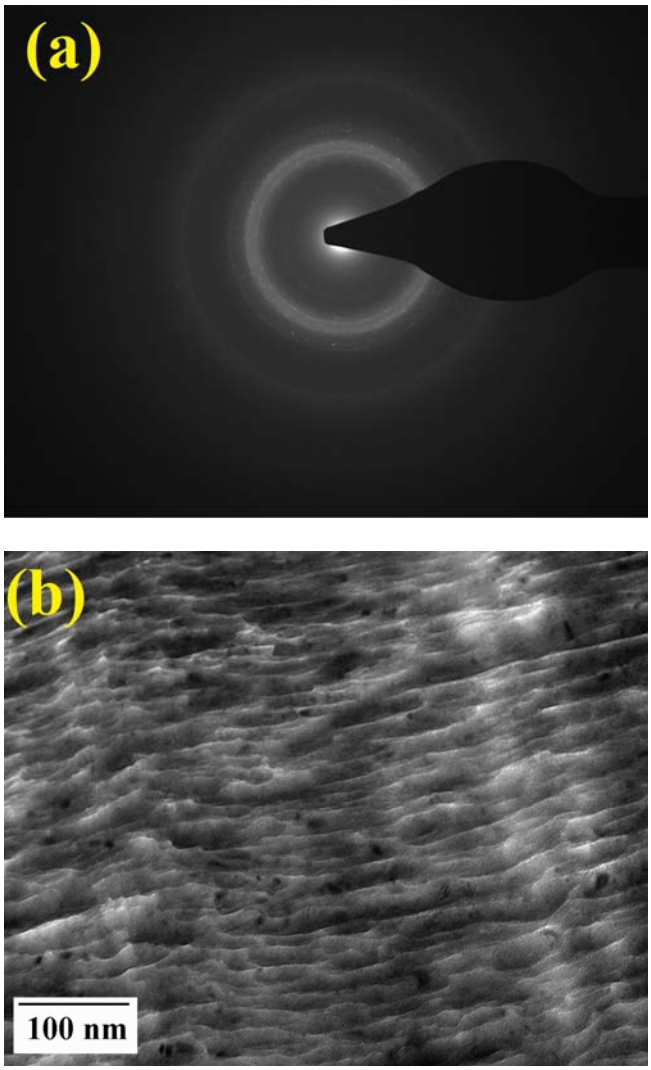

(Figure 6.6. continued)

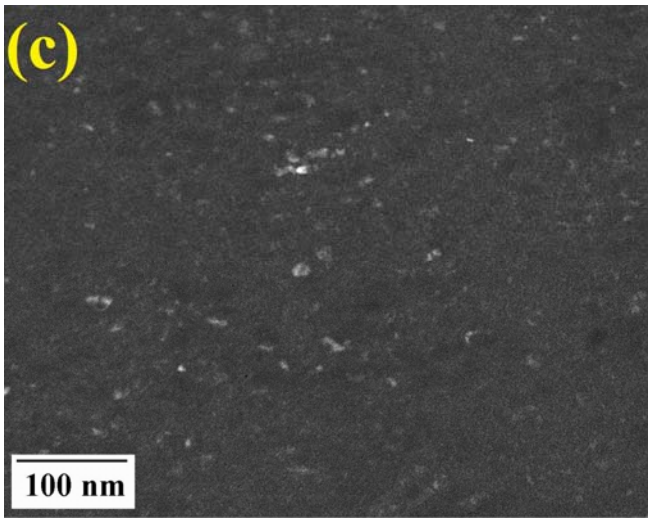

Figure 6-6. TEM images of BMG solder part processed at 300°C, with load of 36.5 N, specimen shown in Figure 6-3(b). (a) spot pattern, (b) bright field image and (c) dark field image of the same place shown in (b). (Magnification: 220,900×)

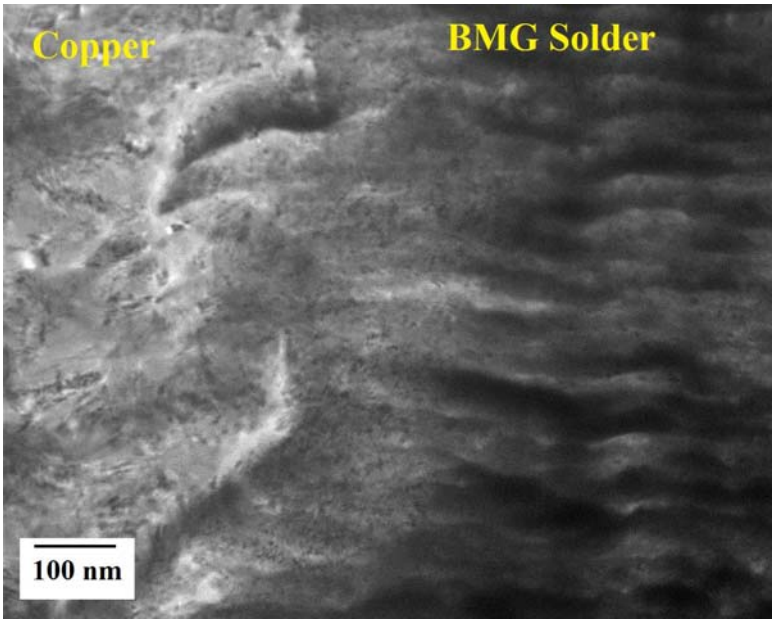

Figure 6-7. Interface between copper substrate and BMG solder in specimen processed at 300°C with 36.5 N load.

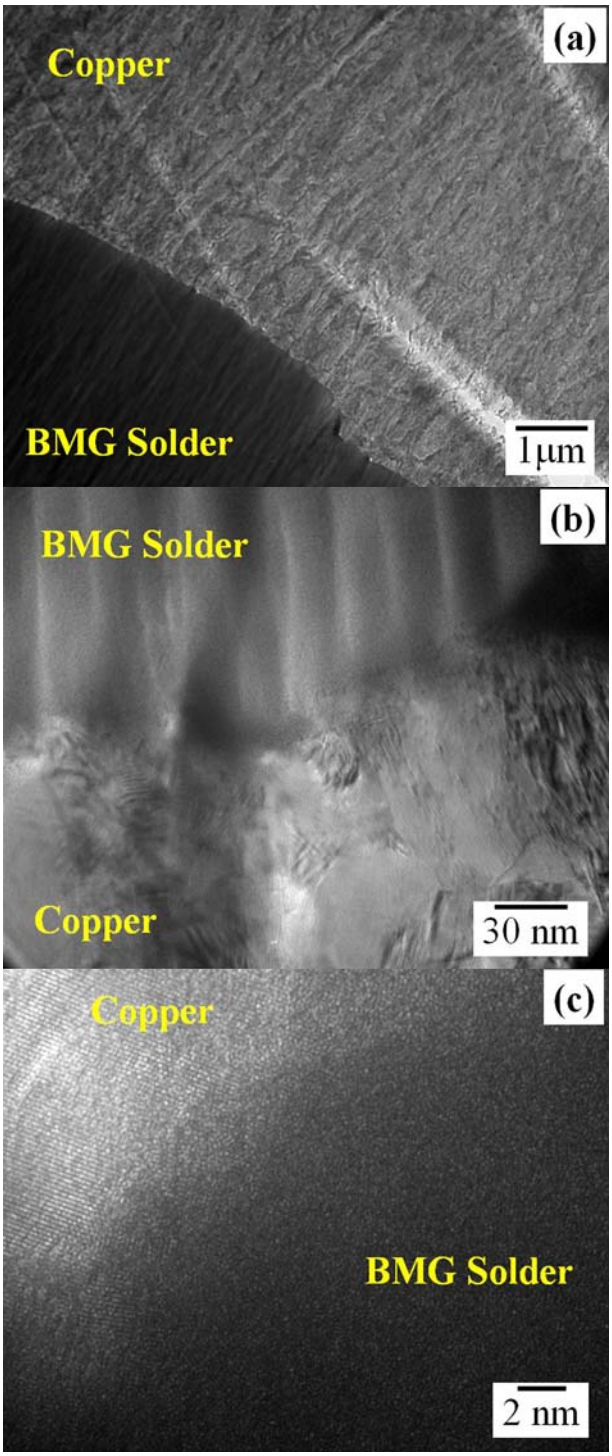

Figure 6-8. The solder-copper interface shown at (a) low magnification (15,400×), (b) high magnification (523,000×) and (c) high resolution (5,335,000×)

6.5 Effect of pressure distribution

Although the viscosity of supercooled liquid can be as low as 6×10^4 Pa·s, similar to that of viscous polymer melts [1], the viscosity of supercooled liquid is still much higher than that of molten tin around the melting point, which is about 2×10^{-3} Pa·s [16]. As a result, pressure needs to be applied during the joining process to assist the supercooled liquid to spread out and wet on other metal surfaces. Pressure dependence on joint quality could exist. However, the fluid pressure squeezed between parallel plates is decreasing as a function of r, distance from center, as described in Equation 6-1 [13].

$$p = -\frac{3\eta}{h^3}\frac{dh}{dt}\left(R^2 - r^2\right) + \Pi \qquad \text{Equation 6-1.}$$

η denotes liquid viscosity, h liquid thickness, t time, R outermost distance of liquid from center and Π constant pressure.

This pressure distribution seems to affect the bonding quality. Figure 6-9 shows cross-sectional image of the rim part of the specimen shown in Figure 6-3(b-2), which is processed at 300°C with 36.5 N of load. Inset of Figure 6-9 is the overall specimen cross-sectional image. Figure 6-9 is taken from the square inside the inset. From the overall cross-sectional image, the machined area which is slanted about 2-3 degree angle to the horizontal and central ‘contact zone’ is clearly seen. At the point where this inclination begins, the boundary between bonding and no-bonding surface exists as can be seen from the magnified image. Thus, the previous observation that the slope outside the ‘contact zone’ causes an additional pressure drop and results in poor bonding quality in this area is confirmed again.

Systematic study carried out in section 6.3 of this chapter shows the existence of required minimum process load for a joint formation. However, the effect of additional load on joint integrity appears to be insignificant once the process load exceeds this critical threshold. The

insensitivity to pressure after exceeding the critical threshold could be due to the open nature of the squeezing geometry. In other words, pressure dependence could exist and be detectable if the flow of the supercooled liquid could be confined. Further refined experiments are required to confirm the effect of pressure.

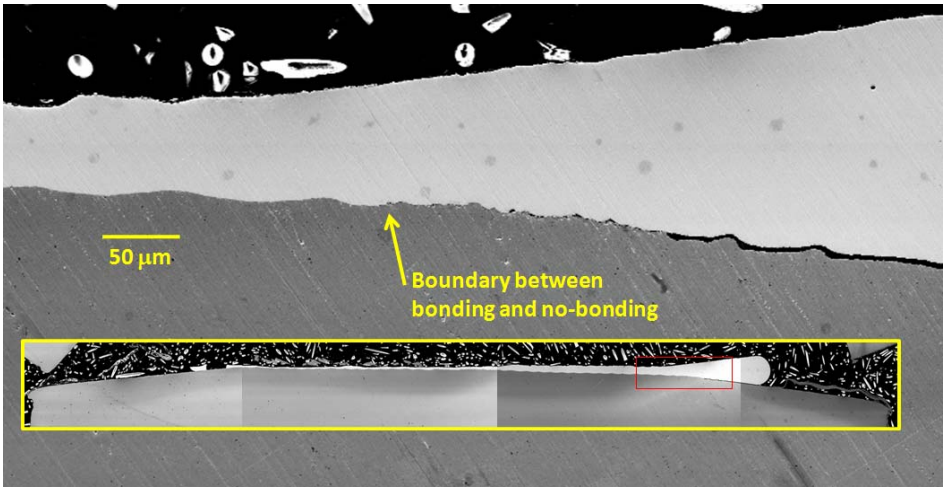

Figure 6-9. Rim part of the specimen shown in Figure 6-3(b-2). Inset: Overall specimen cross-section having small square mark on the right side. This small square is where this figure is taken from.

6.6 Interfacial reaction and fracture behavior

The interface formed by 300°C with a load of 36.5N is magnified in Figure 6-10. The left column of the figures is from the upper part, the boundary between Pt-BMG solder and the molding compound as shown in Figure 6-9, and the right column is from the lower part, the boundary between Pt-BMG solder and the copper substrate. The upper row of the figures is taken by secondary electron detector and the lower row by back-scattered electron (BSE) detector.

Compositional contrast by BSE detector reveals a different phase formed between Pt-BMG and copper substrate, indicated by arrows in Figure 6-10(a-2) and (b-2). This ‘reaction layer’ is also found in the interface formed at 290°C, but is not as pronounced as that of 300°C, as shown in Figure 6-11. This reaction layer makes a clear distinction between the interfaces formed at 290 and 300°C. Temperature appears to be an important factor for formation of the reaction layer. The existence of reaction layer has not been confirmed by TEM yet. But, it should be recalled that this reaction layer is not a necessary condition for intimate bonding interface formation as proven by TEM work shown by Figure 6-8 for a specimen processed under 300°C.

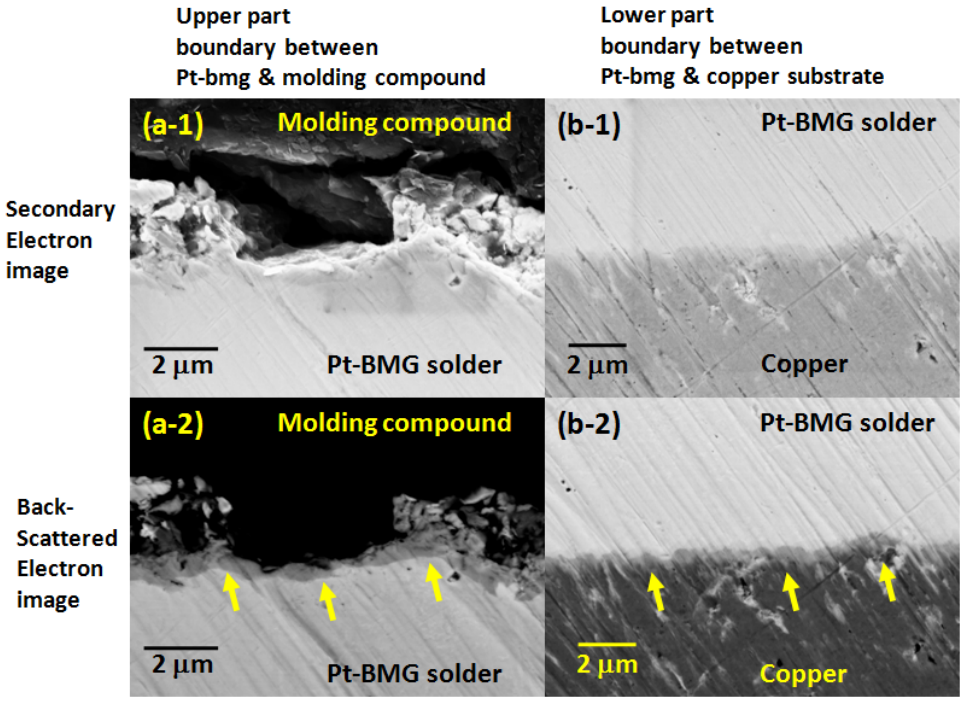

Figure 6-10. Magnified images of interface shown in Figure 6-9 and Figure 6-3(b-2), produced at 300°C with a load of 36.5N. (a) Upper part of the specimen. Boundary between the Pt-BMG solder and molding compound. (b) Lower part of the specimen. Boundary between the Pt-BMG solder and copper substrate. (a-1) and (b-1) are secondary electron images. (a-2) and (b-2) are back-scattered electron images.

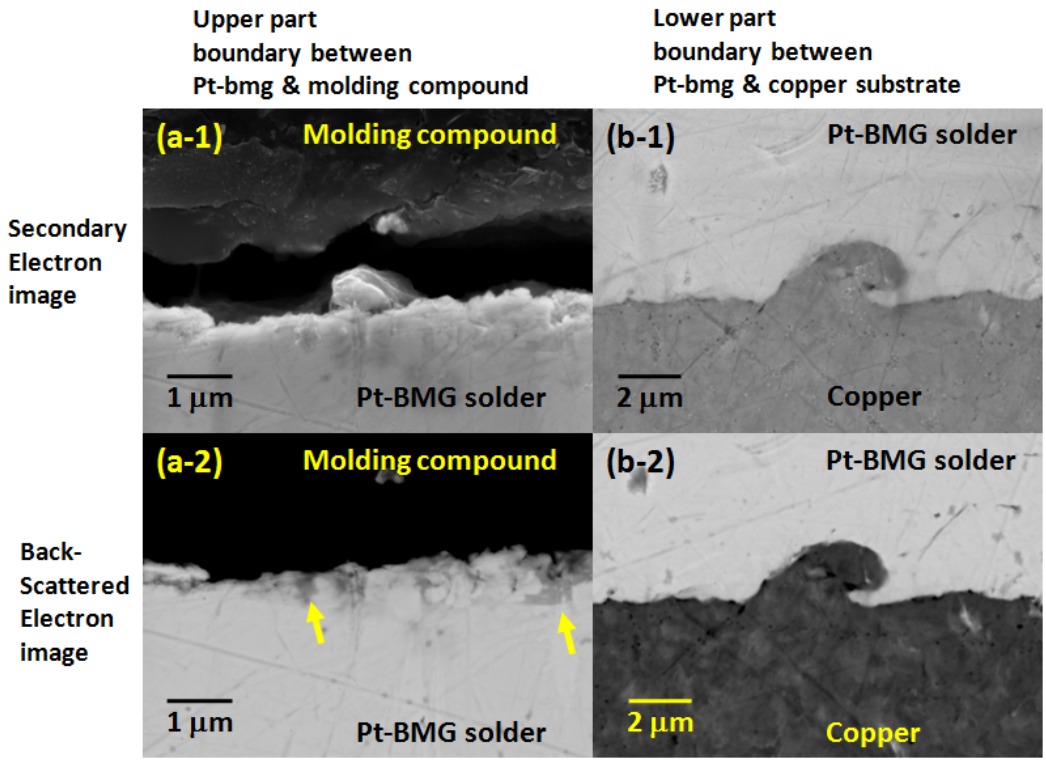

Figure 6-11. Magnified images of interface of the specimen shown in Figure 6-3(a-2), produced at 290°C with a load of 36.5N. (a) Upper part of the specimen. Boundary between the Pt-BMG solder and molding compound. (b) Lower part of the specimen. Boundary between the Pt-BMG solder and copper substrate. (a-1) and (b-1) are secondary electron images. (a-2) and (b-2) are back-scattered electron images.

The interface between the Pt-BMG and the copper substrate of a specimen after a tension test is carefully observed and cavities like the ones shown in Figure 6-12 are found. These cavities appear to be expanded by plastic deformation of the copper substrate following their nucleation. The cavity shown in Figure 6-12(b) in particular, has wedged shape on both the Pt-BMG surface and the copper substrate and the distance between them widens from the tensile load applied to this interface. Some of the cavities have compositional contrast on top, implying

that the top is richer in copper than other parts of the BMG. This suggests a high temperature diffusion process called ‘Kirkendall voiding’ as a possible candidate for void nucleating mechanism. Kirkendall voids are defined as voids induced by a diffusion couple between two different metals that have different interdiffusion coefficients. As shown in Figure 6-3 and Table 6-2, fracture at the interface between the Pt-BMG and copper leaves copper residue on the Pt-BMG surface. This copper residue could be either pure copper pieces pulled from copper substrate or copper atoms diffusing into the Pt-BMG solder. Thus, it is reasonable that such Kirkendall voids nucleate during or after bonding process. However, EDS analysis confirms that interfacial fracture leaves little Pt-BMG residue on the copper surface. Therefore, copper appears to be the only candidate for the possible diffusion process in this system.

The fracture surface of Pt-BMG with high copper concentration (like the area ‘A’ defined in Figure 6-3(b-2)) is observed at higher magnification and compared to matching surface of copper. Figure 6-13 is a direct comparison of two matching fracture surfaces with high magnification. An island full of dimples surrounded by Pt-BMG fracture surface exists. In other words, fracture occurred through Pt-BMG, not along the interface, except for the island area. In the island area, fracture occurred through the interface between Pt-BMG and copper surface. Figure 6-13(a) is a back-scattered electron image and (b) is a secondary electron image. In Figure 6-13(a), Pt-BMG surface underneath the copper residues pulled out by tension loading looks darker than the surrounding Pt-BMG, probably due to higher copper concentration. Dimple patterns in (a) and (b) match in shape, which suggests that the dimple patterns form following the bonding process. If the dimple patterns on the copper surface in Figure 6-13(b) existed before bonding, the Pt-BMG would have generated a negative replication of the dimples during bonding. Thus, it is apparent that the dimple patterns on the copper surface have formed either by Kirkendall void diffusion right after bonding or by heavy deformation during the tension test. In

this sense, Figure 6-13 can be connected to Figure 6-12 in describing possible fracture mechanism of the interface. Figure 6-14 provides the same comparison for another specimen processed at the same temperature, 300°C. Figure 6-14(a) and (b) are matching surfaces but they do not look like matching surfaces. Like Figure 6-13, Pt-BMG solder does not replicate the copper surface, which suggests that both fracture surfaces have formed after the bonding process. It is noteworthy that a magnified view of the Pt-BMG surface in Figure 6-14(c) has distributed compositional contrast. The contrast may have originated from the mixture of original Pt-BMG (white, arrow 'B'), copper diffused Pt-BMG (bright gray, arrow 'A') and copper residue (dark, arrow 'C'). Based on these observations, it is rather clear that the higher copper concentration on the surface of Pt-BMG detached from the copper substrate is a combination of pure copper pieces pulled from copper substrate and copper atoms diffusing into the Pt-BMG solder.

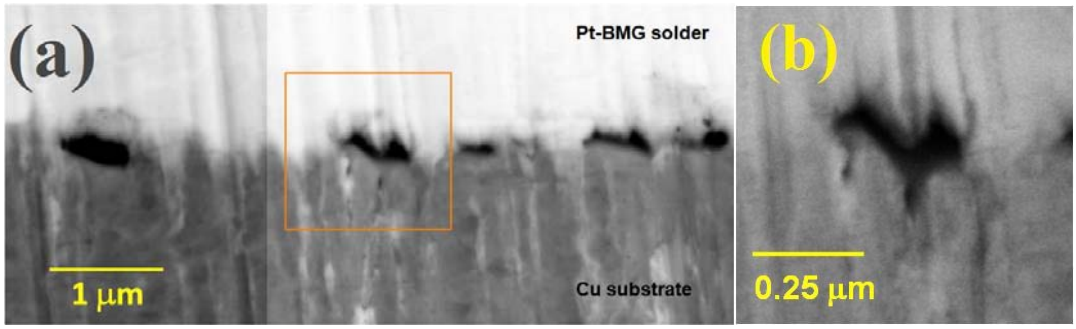

Figure 6-12. (a) Back-scattered electron image of interface between Pt-BMG solder and Cu substrate after tension test, showing cavities nucleated and expanded. (b) magnified secondary electron image of the cavity squared in (a).

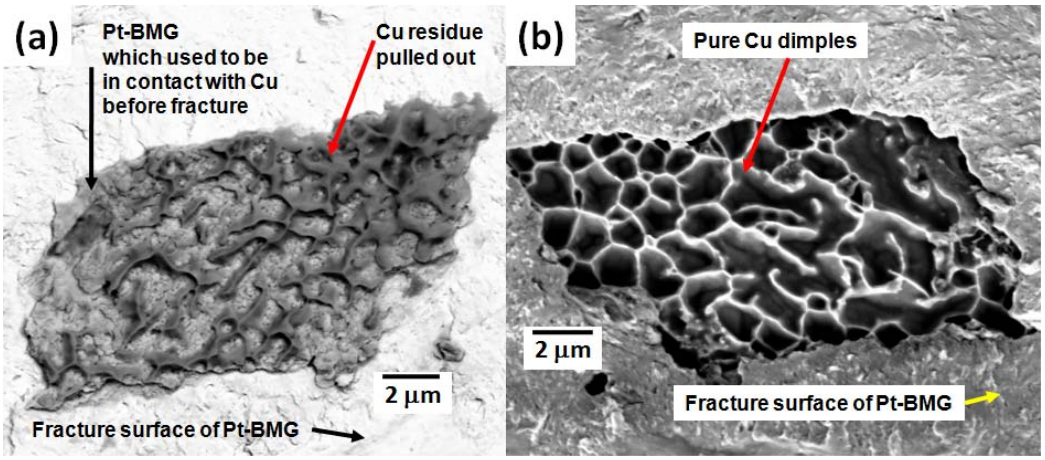

Figure 6-13. Matching fracture surfaces of a joint processed at 300°C. (a) Fracture surface of Pt-BMG side. Central area has copper residue pulled out by tension (b) Exposed pure copper surface surrounded by Pt-BMG residue still sticking to the copper surface.

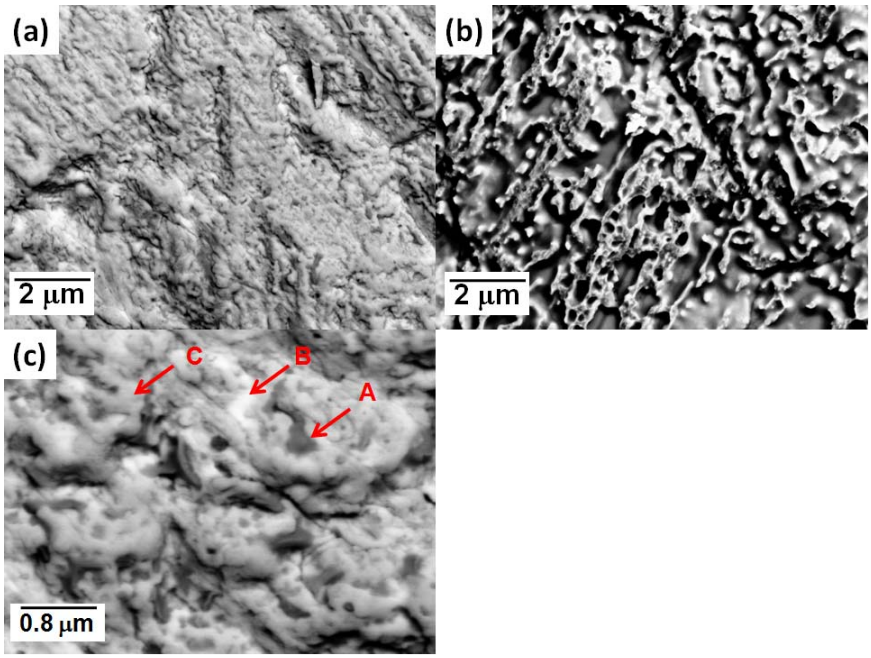

Figure 6-14. Fracture surface of a joint processed at 300°C. All images are taken by back-scattered electron detector. (a) Pt-BMG solder and (b) copper substrate. (c) higher magnification image of Pt-BMG surface showing compositional contrast.

6.7 Applicability of other BMG's

Although Pt-BMG has low glass transition temperature (T_g) comparable to the reflow temperature of conventional soldering in microelectronics industry and is proven successfully to work as a thermoplastic "solder", its optimum process temperature is much higher than T_g, close to the crystallization temperature (T_x). Thus, the next step is to search for other BMG's with lower process temperature available for the thermoplastic joining process. Possible candidate BMG's are Au-based [17], Mg-based [18] and La-based [19] alloys. In this study, $Au_{49}Ag_{5.5}Pd_{2.3}Cu_{26.9}Si_{16.3}$, a variant of $Au_{49}Ag_{5.5}Pd_{2.3}Cu_{26.9}Si_{16.3}$ with Ti addition and $La_{57.6}Al_{17.5}Cu_{12.45}Ni_{12.45}$ alloys are produced and processed for thermoplastic joining. Table 6-3 shows basic data of the alloys used in this study. The addition of Ti has little effect on ΔT or the heat of crystallization. The $Au_{49}Ag_{5.5}Pd_{2.3}Cu_{26.9}Si_{16.3}$ and $Au_{48}Ag_{5.5}Pd_{2.3}Cu_{26.9}Si_{16.3}Ti_1$ alloys do not bond with the pure copper surface. A possible reason is based on the thermal stability. Figure 6-15 shows DSC scans of the $Au_{48}Ag_{5.5}Pd_{2.3}Cu_{26.9}Si_{16.3}Ti_1$ alloy specimens processed at different temperatures for 2 minutes. Specimens processed at 160 and 170°C have almost the same DSC curves as that of an as-cast specimen, which means there is no significant crystallization. These specimens are not fully squeezed out during joining process which implies that the solder does not have enough fluidity. But, once the temperature reaches a critical temperature causing enough fluidity to result in the BMG solder forming a bond, the BMG solder crystallizes. There is no evidence of remaining glass from the specimens processed at 175 and 180°C. This abrupt crystallization behavior contrasts with Pt-BMG solder which still has significant fraction of glass even after a long exposure and deformation around its crystallization temperature. Time-temperature-transformation (TTT) diagram of both BMG's supports the huge difference in thermal stability. As shown in Figure 6-16, the crystallization kinetics of the $Au_{49}Ag_{5.5}Pd_{2.3}Cu_{26.9}Si_{16.3}$ is much faster than that of $Pt_{57.5}Cu_{14.7}Ni_{5.3}P_{22.5}$. Therefore, it is necessary

to have robust glass forming ability and thermal stability to be used as a thermoplastic solder. On the other hand, $La_{57.6}Al_{17.5}Cu_{12.45}Ni_{12.45}$ has higher T_g, T_x and ΔT than Au-based BMG's. A joint processed at 230°C for 2 minutes with 14.2 N of load has about 3 kgf (kilogram-force) of fracture load. Figure 6-17 shows the joint after a tension test. Although the strength of the joint is much smaller than the fracture loads of Pt-BMG joints, 3 kgf of bonding strength suggests a bond formation on a limited area of the contact surface. Further study is required.

Table 6-3. Thermal properties of Au-based and La-based BMG's.

composition (at %)	T_g (°C)	T_x (°C)	ΔT	d_c (mm)	ref.
$Au_{49}Ag_{5.5}Pd_{2.3}Cu_{26.9}Si_{16.3}$	128	186	58	5	[17]
$Au_{48}Ag_{5.5}Pd_{2.3}Cu_{26.9}Si_{16.3}Ti_1$	125.4	182.1	56.7	-	-
$La_{57.6}Al_{17.5}Cu_{12.45}Ni_{12.45}$	162	237	75	8	[19]

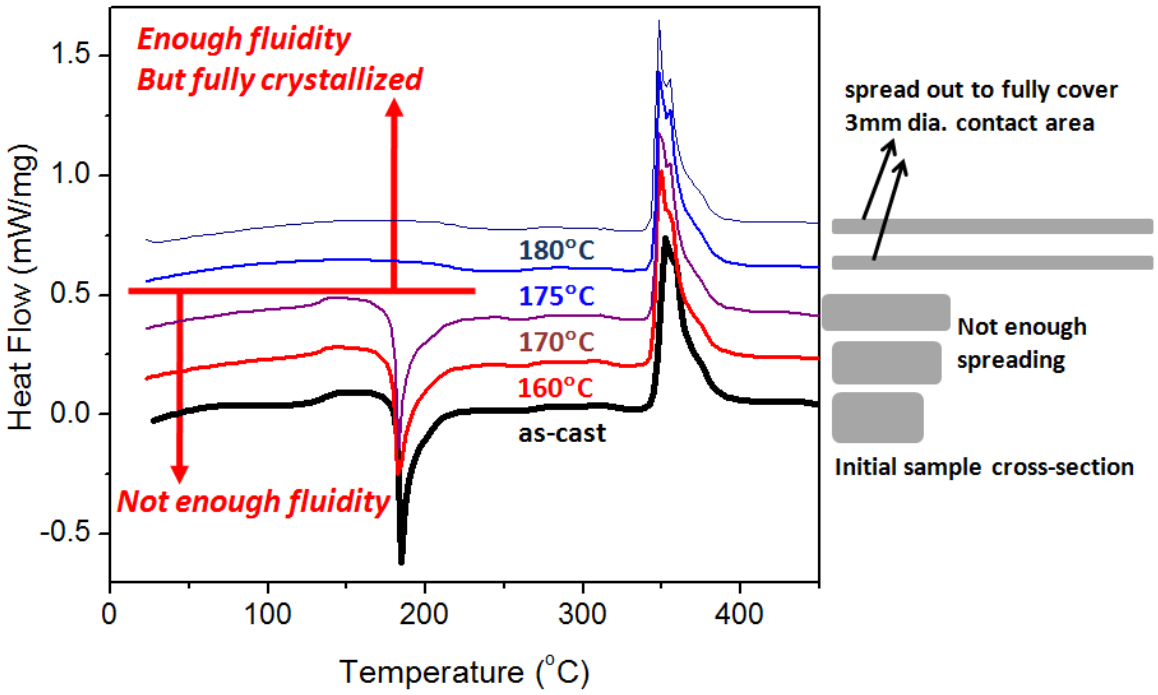

Figure 6-15. DSC scans of the $Au_{48}Ag_{5.5}Pd_{2.3}Cu_{26.9}Si_{16.3}Ti_1$ alloy solder pieces after joining process. Right side of the figure shows cross-sectional shape change of each solder specimen by the process.

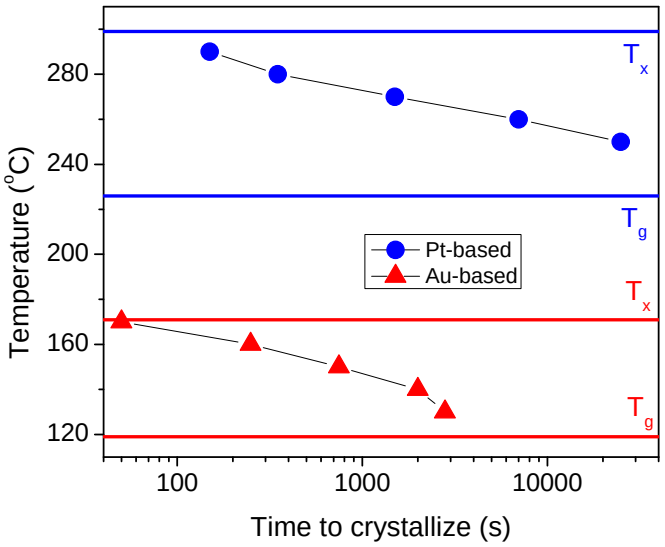

Figure 6-16. Time-temperature-transformation (TTT) diagram of Pt-based and Au-based glasses. Data for Au-based BMG is from Ref. 20 and data for Pt-BMG is from Ref. 21.

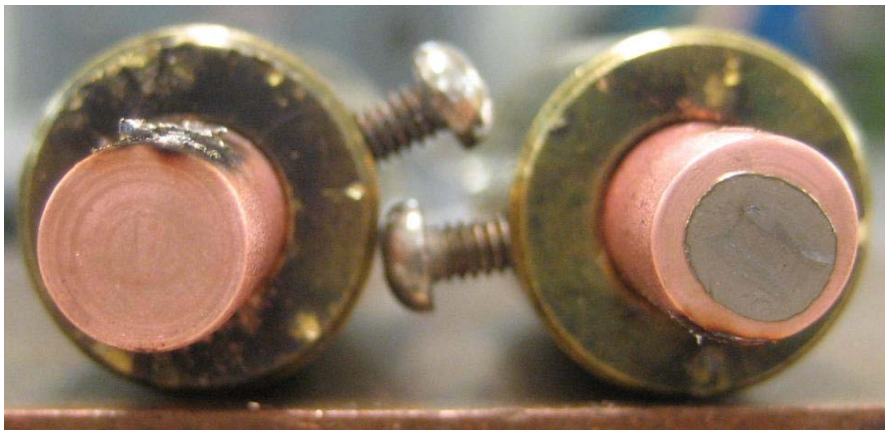

Figure 6-17. La-based BMG joint after tension test (diameter of the copper cylinders is 6.35mm).

Experimental results with Au-, La- and Pt-BMG suggest thermally activated bond formation during atomic configuration rearrangement in the supercooled liquid state. An intimate bond interface between a Pt-BMG and pure copper can be achieved without producing a reaction phase as proven by SEM and TEM work. The bonding mechanism does not appear to require any specific constituent element. Although there is evidence of the diffusion of copper into the Pt-BMG solder, this diffusion process may not be a necessary step; in other words, copper diffusion could be a by-product of the high temperature soldering process, not a crucial process to assist bond interface formation. More study is required to understand the bond forming behavior between pure metal (copper) and BMG.

6.8 Conclusion

In summary, a novel thermoplastic bonding concept was demonstrated using the supercooled liquid region of BMG. With the assistance of a small applied load, the $Pt_{57.5}Cu_{14.7}Ni_{5.3}P_{22.5}$ glassy solder wets a copper surface to form an atomistically-intimate interface. Although there is an evidence of copper diffusion into the Pt-BMG solder by the thermoplastic soldering process, the diffusion is not a necessary condition for bond formation. Fracture of bonding interface proceeds with deformation and subsequent dimple formation of copper. In order to be applicable as a thermoplastic solder, a BMG is required to have a robust glass forming ability and high thermal stability.

Acknowledgements

The authors acknowledge the support from the INTEL Corporation under award No.27940. This work benefited from use of the Caltech KNI and Mat Sci TEM facilities supported by the MRSEC Program of the National Science Foundation under Award Number DMR-0520565.

References

[1] G. Duan, A. Wiest, M.L. Lind, J. Li, W.-K. Rhim and W.L. Johnson, Advan. Mater. 19 (2007) 4272-4275.

[2] J. Schroers, Q. Pham and A. Desai, J. MEMS 16 (2007) 240-247.

[3] T. Laurila, V. Vuorinen and J.K. Kivilahti, Mater. Sci. Eng. R 2005; 49: 1-60.

[4] K. Zeng and K.N. Tu, Mater. Sci. Eng. R 2002; 38: 55-105.

[5] M. Abtew and G. Selvaduray, Mater. Sci. Eng. R 2000; 27: 95-141.

[6] D.W. Kim, D. Suh, T. Millard, H. Kim, C. Kumar, M. Zhu, Y. Xu, Proceedings of IEEE Electronic. Components and Technology Conference 2007; 1614-1619.

[7] D. Suh, C.-w. Hwang, M. Ueshima, J. Sugimoto, Mater. Lett. 2008; 62: 2017-2020.

[8] W.L. Johnson, MRS Bull. 1999; 24(10): 42-56.

[9] F. Ren, J.-W. Nah, K.N. Tu, B. Xiong, L. Xu and J.H.L. Pang, Appl. Phys. Lett. 89 (2006) 141914.

[10] G.Y. Li, B.L. Chen, X.Q. Shi, S.C.K. Wong and Z.F. Wang, Thin Solid Films 504 (2006) 421-425.

[11] J. Schroers and W.L. Johnson, Appl. Phys. Lett. 84 (2004) 3666-3668.

[12] J. Schroers, B. Lohwongwatana, W.L. Johnson and A. Peker, Mater. Sci. Eng. A 449 (2007) 235-238.

[13] G.J. Dienes and H.F. Klemm, J. Appl. Phys. 17 (1946) 458-471.

[14] D. Suh and R.H. Dauskardt, Ann. Chim. Sci. Mat. 27 (2002) 25-40.

[15] X.K. Xi, D.Q. Zhao, M.X. Pan, W.H. Wang, Y. Wu and J.J. Lewandowski, Phys. Rev. Lett. 94 (2005) 125510.

[16] V.H. Stott, Proc. Phys. Soc. 45 (Part1), 530 (1933)

[17] J. Schroers, B. Lohwongwatana, W.L. Johnson and A. Peker, Appl. Phys. Lett. 87 (2005) 061912.

[18] H. Ma, L.L. Shi, J. Xu, Y. Li and E. Ma, Appl. Phys. Lett. 87 (2005) 181915.

[19] H. Tan, Y. Zhang, D. Ma, Y.P. Feng and Y. Li, Acta Mater. 51 (2003) 4551.

[20] Unpublished data of Boonrat Lohwongwatana.

[21] J. Schroers, B. Lohwongwatana, W.L. Johnson and A. Peker, Mat. Sci. Eng. A 449-451 (2007) 235.

Appendix 6-A Coefficient of Thermal Expansion (CTE) of BMG's

Joining two different materials together always accompanies problems caused by the mismatch of Coefficient of Thermal Expansion (CTE). Since the thermoplastic soldering aims microelectronic application, it is required to have knowledge on the CTE of various BMG's to be compared with many other conventional metallic materials. In the Appendix 6-A, the evaluation procedure of CTE of various BMG's are described and discussed.

Thermal expansion measurement is carried out using Perkin Elmer Thermomechanical Analyzer (PE-TMA). Figure 6A-1 is a schematic diagram of the measurement setup. With a probe made of quartz (diameter is 3mm), specimens with diameter larger than that of the quartz probe and with height ranging between 5 and 10 mm are pressed with a small load of 5 or 10 mN. Thermocouple and furnace calibrated with melting of Sn and Pb standard samples surround the specimen and probe. The quartz probe is connected to a Linear Variable Differential Transformer (LVDT) which is calibrated with zero point and 9.36 mm standard sample. Figure 6A-2 shows heating and cooling cycles repeated three times on a high purity copper cylinder with 6.35 mm diameter and 6.09 mm height. Heating and cooling rate is 5 K/min and applied load is 10 mN. Except the first heating curve, all heating and cooling curves are matching, as shown in Figure 6A-2(b). So the five curves except the first heating curve are used for evaluating thermal expansion of each specimen. Derivative of the probe position with temperature is shown in Figure 6A-3. The derivative appears almost constant as temperature increases. With linear fitting of five curves in Figure 6A-2(b), simple estimation of CTE with a reference specimen height at room temperature (25°C) is about 16.5×10^{-6} K^{-1}, which is identical to the known value of pure copper, 16.5×10^{-6} at 25°C [1].

Thermal expansion of various BMG alloys are carried out in the same way. Table 6A-1 and Figure 6A-4 show the linear CTE of various BMG's. Linear CTE's of BMG's are varying

from 9.2 to 19.7×10^{-6} K^{-1} showing large difference between them. Two different Zr-based BMG's have almost identical CTE values. This suggests that thermal expansion of BMG is mainly determined by major alloying element. Indeed, as shown by Table 6A-2 and Figure 6A-5, linear CTE of BMG and major constituting pure metal has a rough linear relationship although there is a difference in how far each alloy deviates from the linear relationship. Also, it is noteworthy that the BMG's thermally expand more than major constituting pure metals.

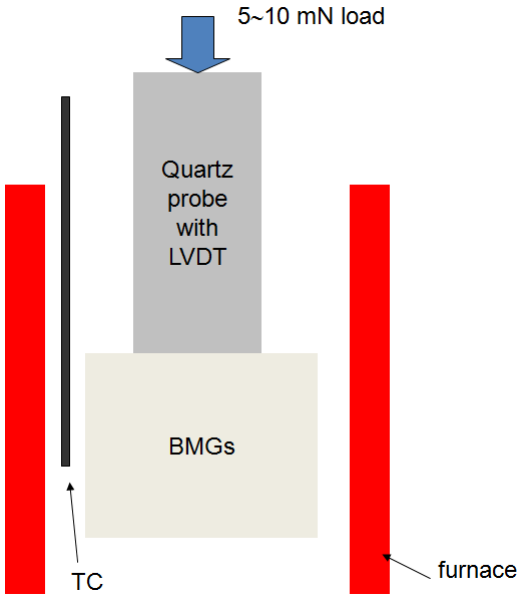

Figure 6A-1. Schematic diagram of CTE measurement setup.

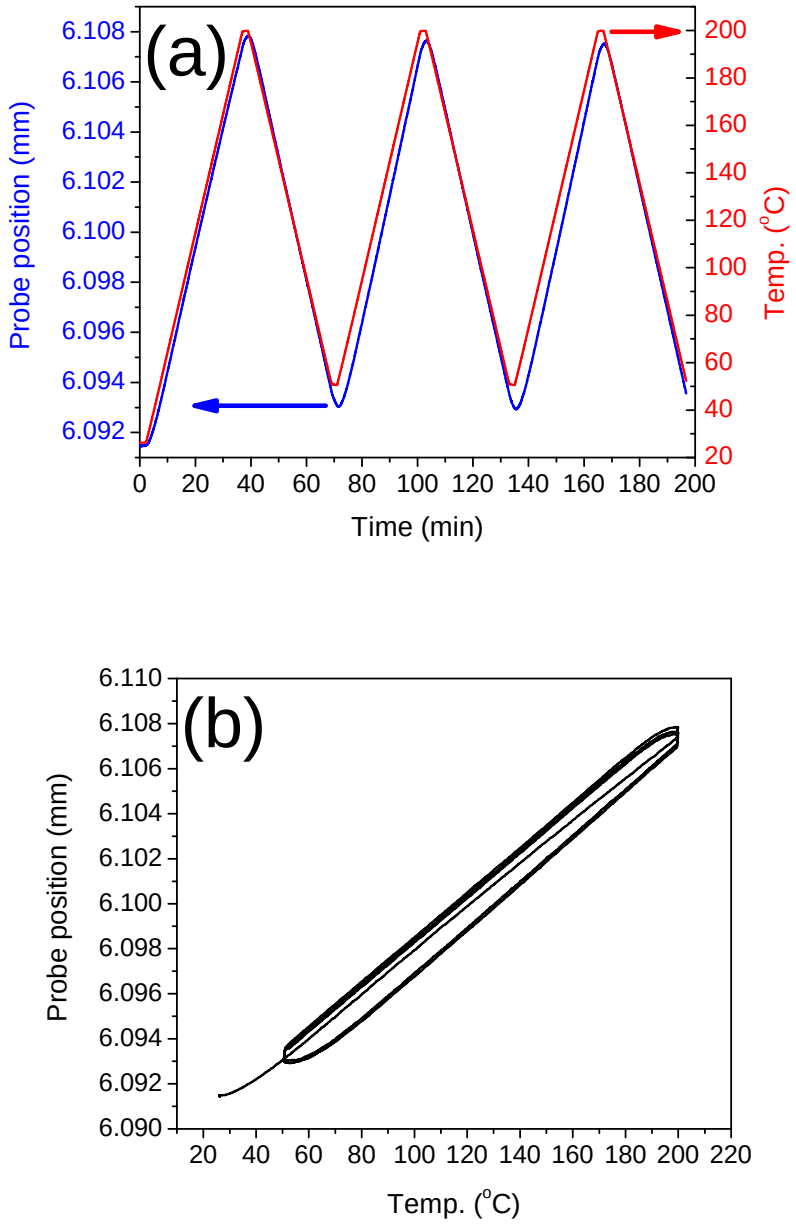

Figure 6A-2. Heating and cooling cycles repeated three times on a high purity copper cylinder with 6.35 mm diameter and 6.09 mm height. (a) Probe position and temperature plotted as a function of time and (b) Probe position as a function of temperature.

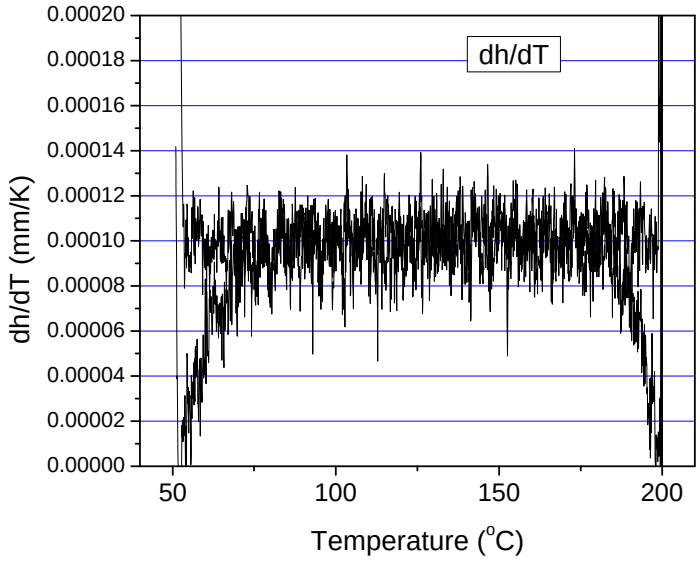

Figure 6A-3. Derivative of probe position by temperature.

Table 6A-1. Linear coefficient of thermal expansion (CTE) of BMG's.

Alloy	Linear CTE (10^{-6} K^{-1})
$Zr_{46.75}Ti_{8.25}Cu_{7.5}Ni_{10}Be_{27.5}$ (Vitreloy 4)	9.2
$Zr_{35}Ti_{30}Cu_{8.25}Be_{26.75}$ (GHDT)	9.3
$Pt_{57.5}Cu_{14.7}Ni_{5.3}P_{22.5}$	10.4
$Pd_{43}Ni_{10}Cu_{27}P_{20}$	14.1
$Au_{49}Ag_{5.5}Pd_{2.3}Cu_{26.9}Si_{16.3}$	19.7

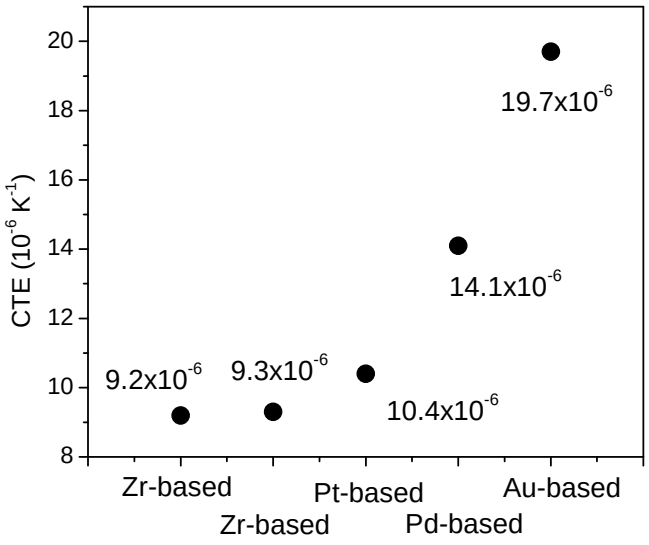

Figure 6A-4. Linear coefficient of thermal expansion (CTE) of BMG's.

Table 6A-2. Linear CTE of pure metals at 25°C [1].

Pure Metal	Linear CTE (10^{-6} K^{-1}) at 25°C
Zr	5.7
Pt	8.8
Pd	11.8
Au	14.2

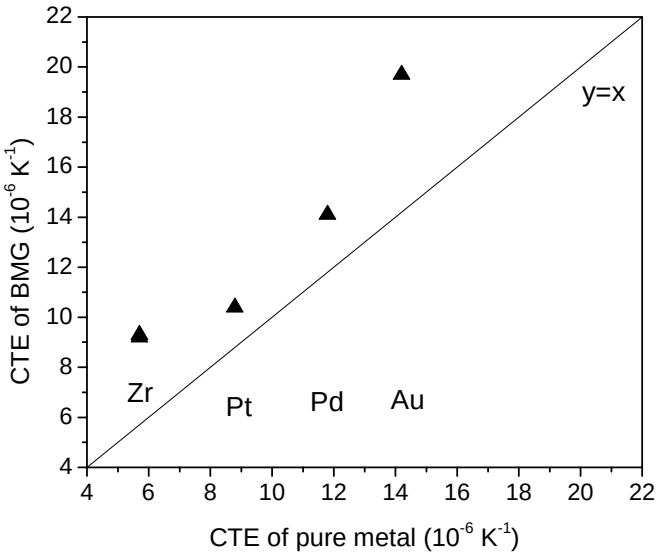

Figure 6A-5. Relationship of CTE's between pure metal and BMG.

Reference for Appendix 6-A

[1] Copper from http://www.wikipedia.org

Appendix 6-B Electrical resistance measurement of BMG's and solder joints

Electrical resistance is used in this chapter as an evaluation parameter on the solder joint interface as shown in Figure 6B-1, because the electrical resistance can provide a sense of how good the interface is as well as the bonding strength does. We can compare the measured resistance value with the ideal resistance of joint calculated by assuming that there is no contact resistance ($R = R_{Cu} + R_{BMG} + R_{Cu}$). In order to evaluate the robustness of a joint, we need to know the electrical resistivity of BMG's first. HP 3468A multimeter and HP 6177 DC current source are used for the typical four point probe setup. A Ni wire with 1mm diameter and 19.5 mm distance between two electrodes for voltage drop measurement is used for verification of the setup. Mean resistance calculated from the data points in Figure 6B-2 is 1.674 mΩ. And the resistivity calculated is $\rho = R\,A/\ell$ =67.4 nΩ·m, which is close to the known value, 69.3 nΩ·m. For a Zr-based BMG (Vitreloy 1, $Zr_{41.2}Ti_{13.8}Cu_{12.5}Ni_{10}Be_{22.5}$), specimen thickness is 2.3 mm and specimen width is 7.88 mm. The distance between two electrodes for voltage drop measurement is 7.7 mm. Mean value for resistance calculated from the data shown in Figure 6B-3 is 0.746 mΩ. And the calculated resistivity is 1756 nΩ·m. In the same way, Pt-based BMG ($Pt_{57.5}Cu_{14.7}Ni_{5.3}P_{22.5}$, 2.32 mm thick × 8.07 mm wide, 6.0 mm distance between two electrodes) has 0.592 mΩ of resistance. Calculated resistivity is 1850 nΩ·m, which is not much different from that of Vitreloy 1.

For the joint shown in Figure 6-3(b-2) and 6-9, the thickness of the squeezed Pt-BMG solder is estimated to be 53 μm in Table 6-1. Actual thickness measured from Figure 6-9 ranges from 46 to 61 μm, having average of about 50 μm at central area. As shown in Figure 6-9, the actual contact area appears almost same as the designed 'contact zone' area. Thus, it looks reasonable to assume the contact area is 7.065 mm^2. Inner probe distance is about 5 mm. Resistance calculated using resistivity of Pt-BMG, 1850 nΩ·m, is 13.1 μΩ. With the contribution

of copper substrate estimated to be around 2.7 μΩ, the total resistance of the joint is 15.8 μΩ. Since there could be a decrease of resistivity of Pt-BMG by partial crystallization, this calculation is likely to underestimate the ideal resistance of the joint. However, the proximity of the measured electrical resistance, 14.7 μΩ, and estimated value, 15.8 μΩ, implies that the formed bonding interface between copper and Pt-BMG has strong intimacy.

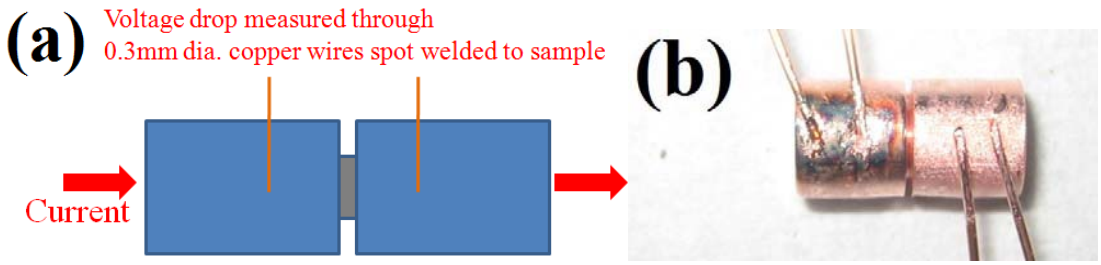

Figure 6B-1. (a) Schematic diagram of electrical resistance measurement performed in this chapter and (b) actual specimen setup.

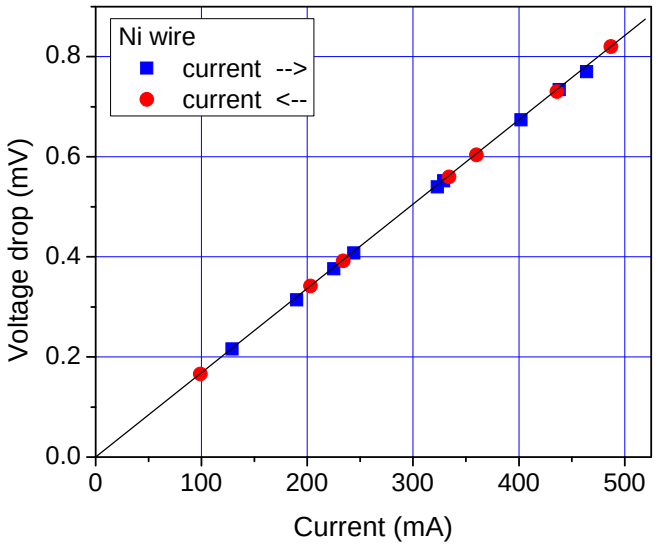

Figure 6B-2. Electrical resistance (Voltage drop) measurement for a Ni wire for verification.

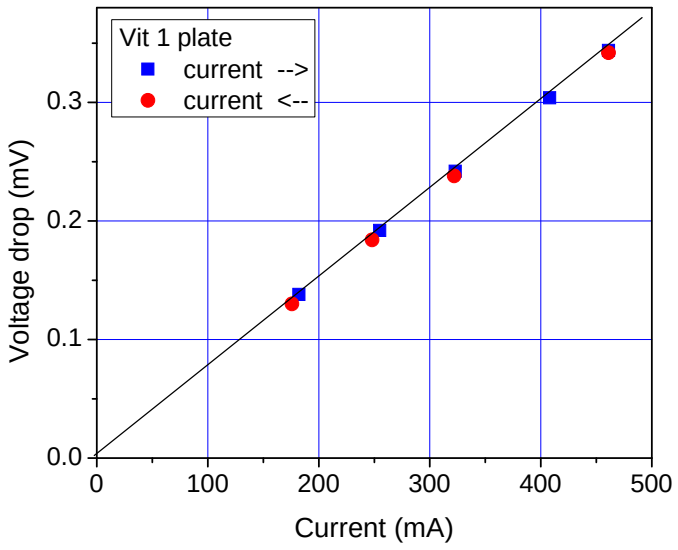

Figure 6B-3. Electrical resistance (Voltage drop) measurement for a Vitreloy 1 plate.

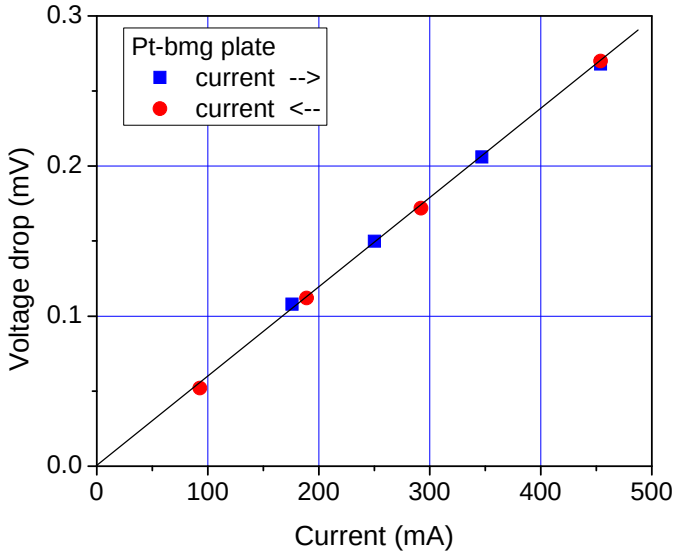

Figure 6B-4. Electrical resistance (Voltage drop) measurement for a Pt-BMG plate.